RIGOROUS COUPLED WAVE ANALYSIS OF RADIALLY AND AZIMUTHALLY-INHOMOGENEOUS, ELLIPTICAL, CYLINDRICAL SYSTEMS

J. M. Jarem

Electrical and Computer Engineering Department
University of Alabama in Huntsville
Huntsville, AL 35899, USA

Abstract—Rigorous Coupled Wave Analysis (RCWA) (used for electromagnetic (EM) analysis of planar diffraction gratings) has been applied to solve EM scattering and diffraction problems for spatially inhomogeneous, cylindrical, elliptical systems. The RCWA algorithm and an appropriate method for matching EM boundary conditions in the elliptical system are described herein. Comparisons of the eigenfunctions determined by RCWA (found in spatially homogeneous elliptical regions) and Mathieu functions are presented and shown to agree closely with one another. Numerical results of scattering from a uniform elliptical shell system (excited by an electrical surface current) obtained by using both a Mathieu function expansion method and by using the RCWA algorithm are presented and also shown to agree closely with one another. The RCWA algorithm was used to study EM scattering and diffraction from an elliptical, azimuthally inhomogeneous dielectric permittivity, step profile system. EM field matching and power conservation were shown to hold for this step profile example. A comparison of the EM fields of the step profile elliptical shell example and that of a uniform profile elliptical shell having the same excitation and bulk material parameters (permittivity and permeability) was made and significant differences of the EM fields of the two systems were observed.

5   Summary and Conclusions

References

1. INTRODUCTION

An important problem in electromagnetics is the problem of determining the EM scattering that arises from a circular or elliptical, cylindrical object whose permittivity and permeability is inhomogeneous, that is, a function of position inside the object. This problem is important, for example in the areas of; dosimetry where one might want to know EM fields levels in biological materials (for example EM field penetration in a limb or torso); terrain clutter where one might want to model EM scattering from cylindrical shaped vegetation (i.e., a tree branch); as exact and approximate solutions to validate other mathematical methods; and many other applications as well.

The problem of EM scattering from radially [1, 2] and azimuthally [3–7] inhomogeneous circular, cylindrical objects has been studied by several authors. Azimuthal, inhomogeneity profile cases have been studied when the object permittivity was a cosine function of ϕ [3–5], when the inhomogeneity profile was a step function [6], when the cylindrical object was inhomogeneous, anisotropic material [7], and in the case when the inhomogeneous scattering object was an approximately circular, cylindrical biological material [8]. The solution method used to study circular, cylindrical inhomogeneous object scattering [6–8] is based on an algorithm called rigorous coupled wave analysis [9–14] which was originally developed to study EM scattering from planar diffraction gratings. The EM RCWA analysis as applied to circular, cylindrical systems was carried out in [6–8] by; (1) solving Maxwell's equation in the interior and exterior regions of the inhomogeneous system in terms of cylindrical Bessel functions, (2) solving Maxwell's equation in the inhomogeneous material region by using a multi-layer state variable (SV) approach, and (3) matching EM boundary conditions at the interfaces. State variable equations arise from using Floquet harmonics (Fourier series) to solve Maxwell's equations in the inhomogeneous material region. The three dimensional problem of EM scattering from a spherical inhomogeneous object has also been studied using RCWA [15, 16]. A recent book [17] has a given a general review of the research work in this area.

A limitation of the circular, cylindrical RCWA method is that the algorithm can only conveniently handle inhomogeneous scattering
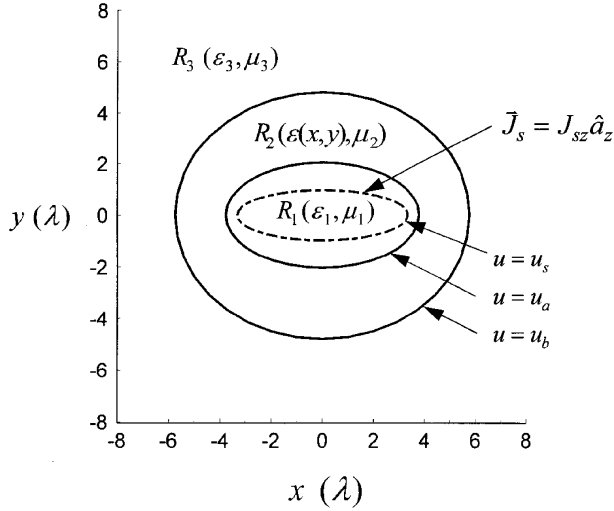
Figure 1. The geometry of the inhomogeneous elliptical system is shown where $\rho = 20$, $u_a = .602$, $u_b = 1.198$, $u_s = .3$, λ is the free space wavelength, and R_1, R_2, R_3 refer to Regs. $1, 2, 3$ respectively. The figure is drawn to scale in the x and y directions. The relative permittivity $\varepsilon(x, y)$ of Reg. 2 is assumed symmetric in the x and y coordinates. For all calculations is assumed: Reg. 1: $\varepsilon_1 = 1.$, $\mu_1 = 1.$; Reg. 3; $\varepsilon_3 = 1.5$, $\mu_3 = 1.2$; and for the uniform profile example it is assumed $\varepsilon(x, y) = \varepsilon_2 \equiv \varepsilon_{2U} = 2.9851786$ and $\mu_2 = 1.4$.

objects which have approximately equal transverse dimensions (i.e., circular or square shaped). In the case when the shape is elongated with even a moderate eccentricity (for example, the elliptical system shown in Figs. 1 and 2) it is difficult to accurately expand the elongated shape in a circular, Fourier series unless an extremely large number of Fourier harmonics are used. Use of a large number of Fourier terms then leads to a large SV matrix which can be difficult and cumbersome to solve. For elongated objects which also have an inhomogeneous permittivity and permeability profiles, a better option is to apply the basic RCWA method using a shape which fits the bulk of the inhomogeneous object as closely as possible.

   With this end in mind. the purpose of this paper is to present a RCWA algorithm which is based on a coordinate system which can fit an elongated inhomogeneous object comfortably, namely the elliptical, cylindrical coordinate system. Figs. 1 and 2 show a schematic of the system to be studied. In Figs. 1 and 2, Regs. 1 and 3 are assumed to
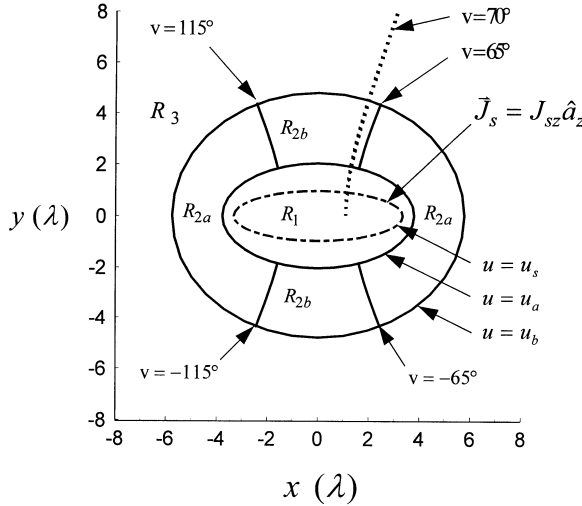
Figure 2. The geometry of the step profile, elliptical system is shown. The relative permittivity step profile is defined by; $\varepsilon(x,y) = \varepsilon_{2a} = 2.95$ in R_{2a}, (Reg. 2a) and $\varepsilon(x,y) = \varepsilon_{2b} = 3.05$ in R_{2a} (Reg. 2b). ε_{2U} has been chosen (see Fig. 1 caption) so $\varepsilon_{2U} = (\varepsilon_{2a}S_{2a} + \varepsilon_{2b}S_{2b})/(S_{2a} + S_{2b})$ where S_{2a} and S_{2b} are the areas of regions of R_{2a} and R_{2b}. All other parameters are specified in the Fig. 1 caption.

be homogeneous. and Reg. 2 is assumed to have a permittivity and permeability profiles which are functions of position.

As an overview of the paper, Sec. 2 of the paper will present the basic elliptical, cylindrical RCWA formulation of the algorithm, Sec. 3 will present an EM field validation solution for the case when all three regions are homogeneous (using Mathieu function expansions), Sec. 4 will present RCWA numerical results for an permittivity step profile (Fig. 2), and Sec. 5 will present conclusions. For simplicity the present paper will present the elliptical RCWA for the case when the inhomogeneity profiles are symmetric in the transverse x, y coordinates and for the case when the exciting EM source is an elliptical, vertically, directed electrical surface current, also assumed symmetric in the transverse x, y coordinates. The extension of the formulation for arbitrary elliptical inhomogeneity profile variation and source excitation is complicated but straight forward.

The study of EM scattering and diffraction from elliptical, cylindrical systems has received a tremendous amount of study in the literature [18, 19]. Reference [18] is a detailed article on scattering

from metallic, elliptical cylinders and also contains a large review of the literature on this subject. A very recent article [19] studies scattering from a spatially uniform, dielectric-coated impedance cylinder.

2. RIGOROUS COUPLED WAVE ANALYSIS FORMULATION

This paper is concerned with the problem of determining the EM fields that arise when an interior, elliptical surface current source (located at $u = u_s, u_s < u_a$) excites EM fields in an elliptical cylindrical system whose permittivity varies with position as shown in Figs. 1 and 2 by using the RCWA method. The EM analysis will be carried out by; (1) solving Maxwell's equations in the interior and exterior homogeneous regions (Regs. 1, 3) of Figs. 1 and 2 in terms of Mathieu functions, (2) solving Maxwell's equation in the inhomogeneous region (Reg. 2) by using a multi-layer state variable approach, and (3) matching EM boundary conditions at the interfaces. It is convenient to use elliptical coordinates as specified in [20] and then normalize them. We let, $\rho = k_0\tilde{\rho}$, $x = k_0\tilde{x}$, $y = k_0\tilde{y}$, $\tilde{x} = \tilde{\rho}\cosh(u)\cos(v)$, $\tilde{y} = \tilde{\rho}\sinh(u)\sin(v)$, etc. where unnormalized coordinates $(\tilde{\rho}, \tilde{x}, \tilde{y},$ etc.) are in meters and $k_0 = 2\pi/\lambda$ is the free space wavenumber (1/meters) and λ is the free space wavelength.

It is assumed that all fields and the inhomogeneity of the medium are z-independent and that the relative dielectric permittivity in an inhomogeneous region of the material system (namely Reg. 2 of Fig. 1) is given by

$$\varepsilon(u, v) = \sum_{i=-\infty}^{\infty} \breve{\varepsilon}_i(u)e^{jiv}, \qquad 0 \le v \le 2\pi$$

where $\breve{\varepsilon}_i(u)$ represent v-exponential, Fourier coefficients.

The EM fields interior (Reg. 1 of Fig. 1) and exterior (Reg. 3 of Fig. 1) when an interior, elliptical surface current source $\vec{J}_s = J_{sz}(u_s, v)\hat{a}_z$ (assumed to be symmetric in both x and y) is present may be expressed as an infinite expansion of radial and angular Mathieu functions [20]. The z-directed electric field and v-directed magnetic field in Reg. 1 are given by

$$E_z^{(1)}(u, v, q_1) = \sum_{m=0,2,...}^{\infty} \left(A_m^{I-} + A_{1m}^{(1)}\right) M_{cm}^{(1)}(u, q_1)ce_m(v, q_1)$$

$$\equiv \sum_{m=0,2,...}^{\infty} E_m^{(1)}(u, q_1)ce_m(v, q_1), \qquad 0 \le u < u_s \qquad (1)$$

$$U_v^{(1)}(u, v, q_1) \equiv \eta_0 h(u, v) H_v^{(1)}(u, v, q_1)$$

$$= \sum_{m=0,2,...}^{\infty} U_m^{(1)}(u, q_1) ce_m(v, q_1)$$

$$U_m^{(1)}(u, q_1) = \frac{1}{j\mu_1} \left(A_m^{I-} + A_{1m}^{(1)} \right) M_{cm}^{(1)'}(u, q_1), \quad 0 \leq u < u_s \qquad (2)$$

$$E_z^{(1)}(u, v, q_1) = \sum_{m=0,2,...}^{\infty} E_m^{(1)}(u, q_1) ce_m(v, q_1),$$

$$E_m^{(1)}(u, q_1) = A_m^{I+} M_{cm}^{(4)}(u, q_1) + A_{1m}^{(1)} M_{cm}^{(1)}(u, q_1), \ u_s \leq u \leq u_a \qquad (3)$$

$$U_v^{(1)}(u, v, q_1) \equiv \eta_0 h(u, v) H_v^{(1)}(u, v, q_1)$$

$$= \sum_{m=0,2,...}^{\infty} U_m^{(1)}(u, q_1) ce_m(v, q_1),$$

$$U_m^{(1)}(u, q_1) = \frac{1}{j\mu_1} \left[A_m^{I+} M_{cm}^{(4)'}(u, q_1) + A_{1m}^{(1)} M_{cm}^{(1)'}(u, q_1) \right], \ u_s < u \leq u_a (4)$$

where $q_1 = \mu_1 \varepsilon_1 \rho^2 / 4$, μ_1 is the relative permeability of Reg. 1, ε_1 is the relative permittivity of Reg. 1, where $\eta_0 = 377\Omega$ is the intrinsic impedance of free space, where the prime denotes differentiation with respect to u and where $h(u, v)$ is the scale factor of elliptical coordinates and is given by [20]

$$h(u, v) = \left(\frac{\rho}{\sqrt{2}} \right) [\cosh(2u) - \cos(2v)]^{1/2} \qquad (5)$$

The amplitude excitation coefficients A_m^{I+} and A_m^{I-} may be found by expanding the source current in a set of orthogonal, angular $ce_m(v, q_1)$ Mathieu functions and then evaluating EM boundary conditions at the location $u = u_s$ of the surface current.

The modal function $\sum_{m=0,2,...}^{\infty} A_{1m}^{(1)} M_{cm}^{(1)} ce_m$ (Eqs. (1), (3)) and its associated derivative (Eqs. (2), (4)) represents the scattered EM field solution of Maxwell's equations in elliptical coordinates which arises in Reg. 1. The modal functions $\sum_{m=0,2,...}^{\infty} A_m^{I-} M_{cm}^{(1)} ce_m$ (Eq. (1)) and $\sum_{m=0,2,...}^{\infty} A_m^{I+} M_{cm}^{(4)} ce_m$ (Eq. (3)) and their associated derivatives, represent respectively, the EM fields which arises inside and outside the current source when the current source is located in an unbounded space having material parameters ε_1, μ_1. The radial Mathieu function $M_{cm}^{(1)}$ has been used in Eqs. (1), (2) because it is bounded at the origin and the radial Mathieu function $M_{cm}^{(4)}$ has been used in Eqs. (3), (4) because it radiates outward from the current source. The radial

Mathieu function $M_{cm}^{(1)}$ is analogous to the circular Bessel function J_m, and the radial Mathieu function $M_{cm}^{(4)}$ is analogous to the circular Hankel-Bessel function $H_m^{(2)}$.

The z-directed electric field and v-directed magnetic field in Reg. 3 are given by

$$E_z^{(3)}(u, v, q_3) = \sum_{m=0,2,\ldots}^{\infty} A_{3m}^{(4)} M_{cm}^{(4)}(u, q_3) ce_m(v, q_3)$$

$$\equiv \sum_{m=0,2,\ldots}^{\infty} E_m^{(3)}(u, q_3) ce_m(v, q_3), \quad u_b \leq u \qquad (6)$$

$$U_v^{(3)}(u, v, q_3) \equiv \eta_0 h(u, v) H_v^{(3)}(u, v, q_3)$$

$$= \frac{1}{j\mu_3} \sum_{m=0,2,\ldots}^{\infty} A_{3m}^{(4)} M_{cm}^{(4)'}(u, q_3) ce_m(v, q_3)$$

$$\equiv \sum_{m=0,2,\ldots}^{\infty} U_m^{(3)}(u, q_3) ce_m(v, q_3) \quad u_b \leq u \qquad (7)$$

where $q_3 = \mu_3 \varepsilon_3 \rho^2/4$, μ_3 is the relative permeability of Reg. 3, ε_3 is the relative permittivity of Reg. 3. Reference [20] gives a complete listing of the Mathieu expansions used subsequently in this paper.

In Region 2, the middle cylindrical dielectric region. we divide the dielectric region into L thin shell layers of thickness Δu_ℓ, $u_b - u_a = \sum_{\ell=1}^{L} \Delta u_\ell$ ($\ell = 1$ is adjacent to $u = u_b$ and $\ell = L$ is adjacent to $u = u_a$) and solve Maxwell's equations in elliptical coordinates by a state variable approach in each thin layer. The layers are assumed to be thin enough in order that the u dependence of $\varepsilon(u, v)$ and the $h(u, v)$ scale factors may be treated as a constant in each layer. Making the substitutions $U_u(u, v) = \eta_0 h(u, v) H_u(u, v)$, and $U_v(u, v) = \eta_0 h(u, v) H_v(u, v)$ where $H_u(u, v)$ and $H_v(u, v)$ represent the magnetic fields in each thin shell region we find that Maxwell's equations in an elliptical, cylindrical shell of coordinate value u are given by

$$\frac{\partial E_z(u, v)}{\partial v} = -j\mu U_u(u, v) \qquad (8)$$

$$\frac{\partial E_z(u, v)}{\partial u} = j\mu U_v(u, v) \qquad (9)$$

$$\frac{\partial U_v(u, v)}{\partial u} - \frac{\partial U_u(u, v)}{\partial v} = j\varepsilon(u, v) h^2(u, v) E_z(u, v) \qquad (10)$$

where μ is the permeability of the thin shell region.

To solve Eqs. (8)–(10), we expand in the Floquet harmonics:

$$E_z(u,v) = \sum_{i=-\infty}^{\infty} S_{zi}(u)e^{jiv},$$

$$U_u(u,v) = \sum_{i=-\infty}^{\infty} U_{ui}(u)e^{jiv},$$

$$U_v(u,v) = \sum_{i=-\infty}^{\infty} U_{vi}(u)e^{jiv},$$

$$\varepsilon_h(u,v)E_z(u,v) = \sum_{i=-\infty}^{\infty} \left[\sum_{i'=-\infty}^{\infty} \breve{\varepsilon}_{h,i-i'} S_{zi'} \right] e^{jiv},$$

$$\varepsilon_h(u,v) \equiv \varepsilon(u,v)h^2(u,v) = \sum_{i=-\infty}^{\infty} \breve{\varepsilon}_{hi}(u)e^{jiv}, \quad (11)$$

If these expansions are substituted in Eqs. (8)–(10), and after letting $\underline{S_z}(u) = [S_{zi}(u)]$, $\underline{U_u}(u) = [U_{ui}(u)]$, and $\underline{U_v}(u) = [U_{vi}(u)]$ be column matrices and $\underline{\underline{\varepsilon_h}(u)} = [\breve{\varepsilon}_{h,i-i'}(u)]$, $\underline{\underline{K}} = [iK\delta_{i,i'}]$, $K = 2\pi/\Lambda_v$, $\Lambda_v = 2\pi(\Lambda_v$ is the elliptical grating period and $\delta_{i,i'}$ is the Kronecker delta) be square matrices we find after manipulation

$$\frac{\partial \underline{V}}{\partial u} = \underline{\underline{A}}\,\underline{V}, \qquad \underline{V} = \begin{bmatrix} \underline{S_z} \\ \underline{U_v} \end{bmatrix}, \qquad \underline{\underline{A}} = \begin{bmatrix} \underline{\underline{A_{11}}} & \underline{\underline{A_{12}}} \\ \underline{\underline{A_{21}}} & \underline{\underline{A_{22}}} \end{bmatrix} \quad (12)$$

where

$$\underline{\underline{A_{11}}} = 0, \quad \underline{\underline{A_{12}}} = j\mu\underline{\underline{I}}, \quad \underline{\underline{A_{21}}} = j\left[\underline{\underline{\varepsilon_h}} - \frac{1}{\mu}\underline{\underline{K}}^2\right], \quad \underline{\underline{A_{22}}} = 0 \quad (13)$$

These equations were obtained after eliminating $\underline{U_u}$ from Eqs. (8)–(10).

Eqs. (12)–(13) represent state variable equations which can determine all possible eigenmodes that exist in each thin layer shell. In the present case, because both the inhomogeneity and the source are assumed symmetric with respect to x and y, only even values of the integer i need to be kept in Eqs. (11)–(13). If Eq. (12) is truncated at order M_T, ($i = -M_T, -M_T + 2, \ldots, M_T - 2, M_T$), ($M_T$ is even), Eq. (12) represents a $N_T = 2(M_T + 1)$ state variable equation (with matrix $(\underline{\underline{A}})_{N_T x N_T}$). The solution of this equation is given by $\underline{V_n}(u) = \underline{V_n} \exp(Q_n u)$ where Q_n and $\underline{V_n}$ are the nth eigenvalue and eigenvector of the constant matrix $\underline{\underline{A}}$ respectively. The quantities $\underline{\underline{A}}$, $\underline{V_n}$, and Q_n satisfy $\underline{\underline{A}}\underline{V_n} = Q_n\underline{V_n}$ where $\underline{V_n}^T = [\underline{S_{zn}}^T, \underline{U_{vn}}^T]$ and

where T represents matrix transpose. The general EM fields in the ℓth thin shell for the nth mode $n = 1, 2, \ldots, N_T$ region are given

$$E_{zn\ell}(u,v) = E_{zn\ell}^e(v) \exp(Q_{n\ell}u)$$

$$E_{zn\ell}^e(v) = \sum_{\substack{i=-M_T \\ (even\ i)}}^{M_T} S_{zin\ell} \exp(jiv), \tag{14}$$

$$U_{vn\ell}(u,v) \equiv \eta_0 h(u,v) H_{vn\ell}(u,v) = U_{vn\ell}^e(v) \exp(Q_{n\ell}u)$$

$$U_{vn\ell}^e(v) = \sum_{\substack{i=-M_T \\ (even\ i)}}^{M_T} U_{vin\ell} \exp(jiv), \qquad n = 1, 2, \ldots, N_T \tag{15}$$

The next general part of the analysis is to match EM boundary conditions at each interface of the system. Before carrying out this numerical procedure, it was decided to initially study the case of scattering from a homogeneous elliptical shell using RCWA (discussed in detail in Sec. 3) and compare this solution to that obtained using a Mathieu function expansion in the elliptical shell. It was felt that this was a good initial step as one could validate the RCWA method and also gain insight into how well the RCWA converged to the correct solution. In comparing numerical results for the homogeneous case, it was found that the propagating eigenmode that had the largest magnitude, eigenvalue (plus and minus roots, $Q_n = \pm j|Q_n|, \mathrm{Real}(Q_n) \cong 0.$), corresponded almost exactly to the $m = 0$ Mathieu function linear combination $[C_0 M_{c0}^{(3)}(u, q_2) + D_0 M_{c0}^{(4)}(u, q_2)]ce_0(v, q_2)$, (with the constants C_0 and D_0 properly chosen), the propagating eigenmode that had the next largest, eigenvalue (plus and minus roots, $Q_n = \pm j|Q_n|, \mathrm{Real}(Q_n) \cong 0.$), corresponded almost exactly to the $m = 2$ Mathieu function linear combination $[C_2 M_{c2}^{(3)}(u, q_2) + D_2 M_{c2}^{(4)}(u, q_2)]ce_2(v, q_2)$, (with the constants C_2 and D_2 properly chosen), and so on, until the eigenfunction magnitudes approached zero and became evanescent. It was also found that in solving the homogeneous case using the Mathieu function expansion, that only a relatively few of the lowest order Mathieu functions $m = 0, 2, 4, \ldots$ were necessary for an accurate solution.

For the reasons that the RCWA eigenfunctions and the Mathieu functions matched closely in the homogeneous case and that only a relatively few Mathieu functions were needed to solve the homogeneous case, it was decided in the present work to consider only elliptical inhomogeneities which are only modestly different from

the homogeneous case. It was expected in this case then that the exact eigenfunctions of the inhomogeneous case would then behave in a similar way numerically as did the RCWA eigenfunctions of the homogeneous case.

With the previous comments and assumptions in mind, we will now proceed with imposing EM boundary at all elliptical interfaces and determining a matrix equation to find all of the unknowns of the system. We begin by expanding the unknown EM RCWA field solution in a thin layer of Reg. 2 of the system in a limited sum of N inward propagating $(Q_n = j|Q_n|, \mathrm{Real}(Q_n) \cong 0, \ n = 1, \ldots, N)$ and N outward propagating $(Q_n = -j|Q_n|, \mathrm{Real}(Q_n) \cong 0, \ n = N + 1, \ldots, 2N)$ RCWA eigenfunctions, and then imposing EM boundary conditions at all interfaces of the system using this expansion. The EM fields in a thin layer of Reg. 2 (Eqs. (14), (15)), is given by

$$E_{z\ell}^{(2)}(u, v) \ = \ \sum_{n=1}^{2N} C_{n\ell} E_{zn\ell}^e(v) \exp(Q_{n\ell}u) \tag{16}$$

$$U_{v\ell}^{(2)}(u, v) \ = \ \sum_{n=1}^{2N} C_{n\ell} U_{vn\ell}^e(v) \exp(Q_{n\ell}u) \tag{17}$$

where in Eqs. (16) and (17), $C_{n\ell}$ are the unknown expansion coefficients of the system.

The next step is evaluate (16) and (17) at each thin layer interface and then impose EM boundary conditions from layer to layer. This has been accomplished by defining the electric field angular functions of Eq. (14) of each thin layer to be weighting functions or testing functions, and then using these weighting functions or testing functions to multiply and integrate the boundary matching equations and thus enforce boundary conditions. The testing or weighting functions for each thin layer were defined to be the inward propagating RCWA electric field eigenmodes, $(Q_n = j|Q_n|, \ \mathrm{Real}(Q_n) \cong 0, \ n = 1, \ldots, N)$, and are given by

$$E_{zn\ell}^t(v) \ \equiv \ E_{zn\ell}^e(v), \qquad n = 1, \ldots, N, \ \ell = 1, \ldots, L \tag{18}$$
$$E_{zn\ell}^t(v) \ \equiv \ E_{znL}^e(v), \qquad n = 1, \ldots, N, \ \ell = L + 1 \tag{19}$$

A testing function $E_{zn,L+1}^t(v)$ has been defined because it will be needed for boundary matching at the Reg. 2, $\ell = L$ and Reg. 1 layer interface.

The boundary testing procedure which has just been described may be called a semi-Galerkin procedure. Using this procedure, one

finds the following equations

$$\sum_{n'=1}^{2N} K_{+,nn'}^{(\ell+1)} C_{n',\ell+1} = \sum_{n'=1}^{2N} K_{-,nn'}^{(\ell)} C_{n',\ell}, \tag{20}$$

for $\ell = 1, \ldots, L-1$, $n = 1, \ldots, 2N$. The interaction terms $K_{+,nn'}^{(\ell+1)}$, $K_{-,nn'}^{(\ell)}$ are given by

$$K_{+,nn'}^{(\ell+1)} = \int_0^{2\pi} E_{zn,\ell+1}^t(v) E_{zn',\ell+1}^e(v) dv \tag{21}$$

$$K_{-,nn'}^{(\ell)} = \left[\int_0^{2\pi} E_{zn,\ell+1}^t(v) E_{zn',\ell}^e(v) dv \right] \exp(-Q_{n'\ell} \Delta u_\ell) \tag{22}$$

for $n = 1, \ldots, N$ and $n' = 1, \ldots, 2N$, and

$$K_{+,nn'}^{(\ell+1)} = \int_0^{2\pi} E_{zn,\ell+1}^t(v) U_{vn',\ell+1}^e(v) dv \tag{23}$$

$$K_{-,nn'}^{(\ell)} = \left[\int_0^{2\pi} E_{zn,\ell+1}^t(v) U_{vn',\ell}^e(v) dv \right] \exp(-Q_{n'\ell} \Delta u_\ell) \tag{24}$$

for $n = n+1, \ldots, 2N$ and $n' = 1, \ldots, 2N$.

Defining for $\ell = 1, \ldots, L-1$, two $2N \times 2N$ size matrices, $\underline{\underline{K_+^{(\ell+1)}}} = \left[K_{+,nn'}^{(\ell+1)} \right]$ and $\underline{\underline{K_-^{(\ell)}}} = \left[K_{-,nn'}^{(\ell)} \right]$ and defining a $2N$ size column matrix $\underline{C_\ell} = [C_{n\ell}]$, and after matrix inversion of $\underline{\underline{K_+^{(\ell+1)}}}$, it it found

$\underline{C_{\ell+1}} = \underline{\underline{K^{(\ell+1)}}} \underline{C_\ell}$ where $\underline{\underline{K^{(\ell+1)}}} = \left[\underline{\underline{K_+^{(\ell+1)}}} \right]^{-1} \left[\underline{\underline{K_-^{(\ell)}}} \right]$. If successive substitution of each layer column matrix $\underline{C_\ell}$ is made it is found that the $\underline{C_L}$ column matrix may be expressed in terms of the first layer column matrix as

$$\underline{C_L} = \underline{\underline{K^{(L)}}} \, \underline{\underline{K^{(L-1)}}}, \ldots, \underline{\underline{K^{(2)}}} \, \underline{C_1} \equiv \underline{\underline{M}} \, \underline{C_1} \tag{25}$$

It is also necessary to match boundary conditions at the Reg. 3-Reg. 2 and the Reg. 1-Reg. 2 interfaces. At the Reg. 3: (Reg. 2, $\ell = 1$) interface after enforcing the boundary conditions using the testing function set $E_{zn,1}^t(v)$ $n = 1, \ldots, N$ it is found

$$\underline{\underline{K_+^{(1)}}} \, \underline{C_1} = \underline{V^{(3)}} \equiv \left[\left(\underline{E_z^{(3)}} \right)^T, \left(\underline{U_z^{(3)}} \right)^T \right]^T \tag{26}$$

where $\underline{\underline{K_+^{(1)}}}$ is given by Eqs. (21), (23) with ℓ set to zero and where

$$\underline{E_z^{(3)}} = \left[E_{zn1}^{(3)} \right], \qquad E_{zn1}^{(3)} = \sum_{m=0,2,\ldots}^{2(N-1)} \beta_{n,m} E_m^{(3)}(u_b, q_3),$$

$$\underline{U_v^{(3)}} = \left[U_{vn1}^{(3)}\right], \qquad E_{zn1}^{(3)} = \sum_{m=0,2,\ldots}^{2(N-1)} \beta_{n,m} U_m^{(3)}(u_b, q_3),$$

$$\beta_{n,m} = \int_0^{2\pi} E_{zn,1}^t(v) ce_m(v, q_3) dv \qquad (27)$$

At the (Reg. 2, $\ell = L$): Reg. 1 interface, after enforcing the boundary conditions using the testing function set $E_{zn,L+1}^t(v)$, $n = 1, \ldots, N$, it is found

$$\underline{V^{(1)}} \equiv \left[\left(\underline{E_z^{(1)}}\right)^T, \left(\underline{U_v^{(1)}}\right)^T\right]^T = \underline{\underline{K_-^{(L)}}}\, \underline{C_L} \qquad (28)$$

where $\underline{\underline{K_-^{(L)}}}$ is defined by Eqs. (22) and (24) with $\ell = L$ and Δu_L set to zero, where

$$\underline{E_z^{(1)}} = \left[E_{zn,L+1}^{(1)}\right], \qquad E_{zn,L+1}^{(1)} = \sum_{m=0,2,\ldots}^{2(N-1)} \alpha_{n,m} E_m^{(1)}(u_a, q_1),$$

$$\underline{U_v^{(1)}} = \left[U_{vn,L+1}^{(1)}\right], \qquad U_{vn,L+1}^{(1)} = \sum_{m=0,2,\ldots}^{2(N-1)} \alpha_{n,m} U_m^{(1)}(u_a, q_1),$$

$$\alpha_{n,m} = \int_0^{2\pi} E_{zn,L+1}^t(v) ce_m(v, q_1) dv \qquad (29)$$

We note that in the numerical evaluation of Eqs. (18)–(29), that all of the angular integrals, that are defined over the period $0 \le v \le 2\pi$ and have the form

$$I = \int_0^{2\pi} f(v)g(v)dv \quad \text{where} \quad f(v) = \sum_{i'=-\infty}^{\infty} \check{f}_{i'} \exp(ji'v) dv$$

$$\text{and} \quad g(v) = \sum_{i''=-\infty}^{\infty} \check{g}_{i''} \exp(ji''v) dv \qquad (30)$$

may be evaluated exactly and have the value $I = 2\pi \sum_{i=-\infty}^{\infty} \check{f}_i \check{g}_{-i}$.

Inverting $\underline{\underline{K_+^{(1)}}}$ of Eq. (26) and inverting $\underline{\underline{K_-^{(L)}}}$ of Eq. (28), one finds

$$\underline{C_1} \left[\underline{\underline{K_+^{(1)}}}\right]^{-1} \underline{V^{(3)}}, \underline{C_L} = \left[\underline{\underline{K_-^{(L)}}}\right]^{-1} \underline{V^{(1)}} \qquad (31)$$

If $\underline{C_1}$ and $\underline{C_L}$ of are now substituted in Eq. (25) we have

$$\left[\underline{\underline{K_-^{(L)}}}\right]^{-1} \underline{V^{(1)}} = \underline{\underline{M}} \left[\underline{\underline{K_+^{(1)}}}\right]^{-1} \underline{V^{(3)}} \qquad (32)$$

The $\underline{V}^{(1)}$ column matrix of Eqs. (28), (29), involves the Reg. 1 coefficient terms $E_m^{(1)}(u_a, q_1)$ and $U_m^{(1)}(u_a, q_3)$ which are given in Eqs. (3), (4) and the $\underline{V}^{(3)}$ column matrix of Eqs. (26), (27) involves the Reg. 3 coefficient terms $E_m^{(3)}(u_b, q_3)$ and $U_m^{(3)}(u_b, q_3)$ which are given in Eqs. (6), (7). If one substitutes $E_m^{(1)}(u_a, q_1)$, $U_m^{(1)}(u_a, q_1)$, $E_m^{(3)}(u_b, q_3)$, and $U_m^{(3)}(u_b, q_3)$ of Eqs. (3), (4), (6), (7) in Eq. (32), and separates the known source terms (proportional to A_m^{I+}) from the unknown EM field expansion terms (proportional to $A_{1m}^{(1)}$ and $A_{3m}^{(1)}$), one finds a final matrix equation which may be solved to find the unknown coefficients $A_{1m}^{(1)}$ and $A_{3m}^{(4)}$, $m = 0, 2, \ldots, 2(N-1)$ of the system. Once the coefficients $A_{1m}^{(1)}$ and $A_{3m}^{(4)}$, $m = 0, 2, \ldots, 2(N-1)$ have been found. all other EM field quantities may also be determined.

3. MATHIEU FUNCTION VALIDATION SOLUTION

As mentioned earlier, an important issue is validating the RCWA elliptical calculations of Sec. 2 using an independent numerical method. This has been accomplished by using Mathieu functions to calculate the EM fields that arise from the elliptical cylinder system shown in Fig. 1 when Reg. 2 is assumed to be a uniform dielectric material of relative permittivity value ε_2. The basic method consists of expanding the EM fields in Regs. 1, 2, and 3 in terms of a finite number $m = 0, 2, \ldots, 2(N-1)$ of radial and angular Mathieu functions which meet proper boundary conditions, and then boundary matching these solutions at the interfaces of Reg. 1–Reg. 2 and Reg. 2–Reg. 3. Because this method is to be directly compared to the RCWA method, the integer N is assumed to the same as is used for the RCWA analysis. The Mathieu function expansions of Regs. 1 and 3 have already been given in Eqs (1)–(7) assuming truncation at order $2(N-1)$. The Mathieu function expansion for Reg. 2 is given by

$$E_z^{(2)}(u, v, q_2) = \sum_{m=0,2,\ldots}^{2(N-1)} E_m^{(2)}(u, q_2) ce_m(v, q_2),$$

$$E_m^{(2)}(u, q_2) = A_{2m}^{(3)} M_{cm}^{(3)}(u, q_2) + A_{2m}^{(4)} M_{cm}^{(4)}(u, q_2), \quad u_a \leq u \leq u_b \ (33)$$

$$U_v^{(2)}(u, v, q_2) \equiv \eta_0 h(u, v) H_v^{(2)}(u, v, q_2)$$

$$= \sum_{m=0,2,\ldots}^{2(N-1)} U_m^{(2)}(u, q_2) ce_m(v, q_2),$$

$$U_m^{(2)}(u, q_2) = \frac{1}{j\mu_2} \left[A_{2m}^{(3)} M_{cm}^{(3)\prime}(u, q_2) + A_{2m}^{(4)} M_{cm}^{(4)\prime}(u, q_2) \right]$$

$$u_a \le u \le u_b \quad (34)$$

$q_2 = \mu_2 \varepsilon_2 \rho^2 / 4$, μ_2 is the relative permeability of Reg. 2, ε_2 is the relative permittivity of Reg. 2, and where $M_{cm}^{(3)}(u, q_2)$ and $M_{cm}^{(4)}(u, q_2)$ represent incoming and outgoing radial Mathieu functions [20]. The boundary matching has been accomplished by; (1) evaluating the EM fields Eqs. (1)–(7) and Eqs. (33)–(34) at the interfaces u_a and u_b; (2) multiplying the resulting equations by a set of angular weighting or testing functions, and (3) integrating the resulting equations over the interval $0 \le v \le 2\pi$. In the present application the weighting or testing functions were taken to be the angular Mathieu functions $ce_m(v, q_2)$.

The result of this operation was a $4N \times 4N$ nondiagonal (and in general nonsymmetric), matrix equation from which all of the $4N$ unknowns $A_{1m}^{(1)}$, $A_{2m}^{(3)}$, $A_{2m}^{(4)}$, $A_{3m}^{(4)}$, $m = 0, 2, \ldots, 2(N-1)$ of the system could be determined. The $4N \times 4N$ matrix equation is nondiagonal (and in general nonsymmetric), because the angular Mathieu functions $ce_m(v, q_2)$ are not in general orthogonal to $ce_m(v, q_1)$ or $ce_m(v, q_3)$ when $q_2 \ne q_1$ or $q_2 \ne q_3$. Once the $4N$ unknowns of the system are determined, it is then possible to evaluate all of the EM fields of the system anywhere in space.

4. NUMERICAL RESULTS

This section will present numerical examples of EM scattering from a uniform elliptical cylinder shell as obtained by using Mathieu functions and obtained by RCWA and will also present examples of EM scattering from a non-uniform, step-profile elliptical cylinder shell as obtained by the RCWA method. The purpose of presenting Mathieu and RCWA numerical results for a uniform elliptical cylinder will be to validate the numerical results of the RCWA method.

The uniform and step profile elliptical cylinder shell examples to be studied are illustrated in Figs. 1 and 2 and consists of a three elliptical regions all assumed to have $\rho = 20$ which are excited by a non uniform surface current source located in Reg. 1 of the system. Figs. 1 and 2 which are drawn to scale in the x and y directions, show the homogeneous (homogeneous when $\varepsilon(x, y) = \varepsilon_2 = $ constant in Fig. 1) and inhomogeneous elliptical cases under consideration. In these figures λ is the free space wavelength and R_1, R_2, R_3, R_{2a}, and R_{2b} refer to the Regs. 1, 2, 3, 2a, and 2b respectively. For both of these examples it is assumed that the region interfaces are located at $u = u_a = .602$ (Reg. 1-Reg. 2), and $u = u_b = 1.198$ (Reg. 2-Reg. 3) and it is also

assumed that the material parameters of Regs. 1, 3 respectively, have the permittivity and permeability values: Reg. 1; $\varepsilon_1 = 1.$, $\mu_1 = 1.$: and Reg. 3; $\varepsilon_3 = 1.5$, $\mu_3 = 1.2$. As can be seen from Figs. 1 and 2, the outer dimensions of the elliptical objects are approximately $12\lambda \times 10\lambda$. In Reg. 2 of the uniform profile example (illustrated in Fig. 1) it is assumed that Reg. 2 has the relative permittivity and permeability parameters $\varepsilon(x,y) = \varepsilon_2 \equiv \varepsilon_{2U} = 2.9851786$ and $\mu_2 = 1.4$ and in Reg. 2 of the step profile example (illustrated in Fig. 2) it is assumed that the regions making up the step have permittivity and permeability parameters: Reg. 2a; $\varepsilon_{2a} = 2.95$, $\mu_2 = 1.4$; and Reg. 2b $\varepsilon_{2b} = 3.05$, $\mu_2 = 1.4$. In the step profile example, Reg. 2a (labeled R_{2a}) is defined by the coordinates $u_a \leq u \leq u_b$, $-65° \leq v \leq 65°$ and $115° \leq v \leq 245°$ and the Reg. 2b (labeled R_{2b}) is defined by the coordinates $u_a \leq u \leq u_b$, $65° \leq v \leq 115°$ and $245° \leq v \leq 295°$. The dielectric permittivity of the step profile is symmetric in the x and y directions. In the uniform profile example the value of the relative dielectric permittivity $\varepsilon(x,y) = \varepsilon_2 \equiv \varepsilon_{2U} = 2.9851786$ was chosen so that its value exactly equaled the average or bulk value of the step profile case. In other words if S_{2a} and S_{2b} represent the total areas of regions of R_{2a} and R_{2b} then $\varepsilon_{2U} = \frac{\varepsilon_{2a}S_{2a} + \varepsilon_{2b}S_{2b}}{S_{2a} + S_{2b}}$. The bulk values of the uniform and step profile cases were chosen to be equal in order to ensure that a more meaningful comparison of the EM fields and powers of a homogeneous and inhomogeneous case could be made. A difference in the EM fields or powers tor two cases due to a difference in the dielectric permittivity bulk parameters in each case, would not represent an EM field difference due to the elliptical shell being homogeneous or inhomogeneous. For both the homogeneous and inhomogeneous examples it is assumed that the excitation surface current is given by

$$\vec{J}_S(u_s, v) = J_{s0}ce_0(v, q_1)/h(u_s, v)\hat{a}_z \qquad (35)$$

where $h(u_s, v)$ is the elliptical scale factor and is given in Eq. (5) and $ce_0(v, q_1)$ is an angular Mathieu function of order $m = 0$. By matching EM boundary conditions at the current source location it can be shown mathematically that the current source of Eq. (35) will only excite a $m = 0$ Mathieu function mode in a uniform, infinite region of space. For both examples to be presented, the surface current amplitude J_{s0} was chosen to have a value $J_{s0} = 1.$ (Amp/m) and the surface current was assumed to be located at $\rho = 20$, $u = u_s = .3$. The number of thin layers L used to make all RCWA calculations was results for both the uniform and step profile examples calculations in this paper was $L = 298$. All RCWA eigenfunctions were calculated using a truncation value of $M_T = 32$ in Eqs. (12), (13). The parameter N was chosen
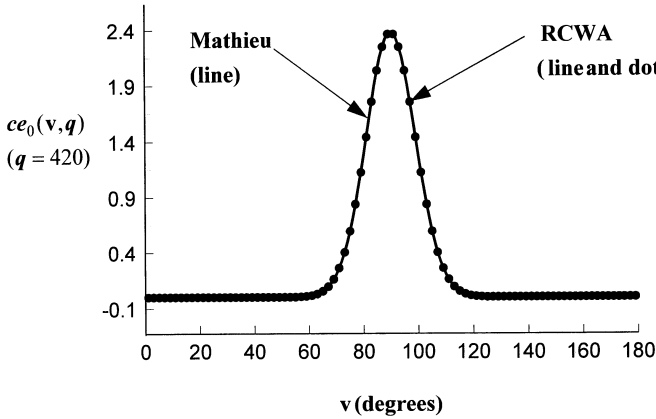
Figure 3. A comparison of the $ce_0(v, q)$ angular Mathieu function (*line*) as obtained by the numerical algorithm of [21] and as obtained by the RCWA algorithm for $q = 420$. This value of $q(q = \mu\varepsilon\rho^2/4)$ would correspond to the case when $\rho = 20$, $\mu = 1.4$, $\varepsilon = 3$.

to have a value of $N = 12$ for numerical results to be presented. All Mathieu function calculations in the paper were made using the numerical algorithm of [21].

We will now present numerical results of the $m = 0$ angular and radial Mathieu functions which were obtained using the RCWA method and compare these to the Mathieu functions obtained from [20, 21] for the case when the parameter q was taken to be $q = 420$. This value of q corresponds to the case when Reg. 2 of Figs. 1 or 2 is a uniform elliptical shell ($\rho = 20$ in Reg. 2) and $\varepsilon(x, y) = \varepsilon_2 = 3.$, $\mu_2 = 1.4$. Fig. 3 shows a plot of the of the Reg. 2 $ce_0(v, q)$ angular Mathieu function (*line*) as obtained by the numerical algorithm of [21] and as obtained by the RCWA algorithm (*line and dot*). Figs. 4 and 5 show respectively the Reg. 2, $M_{c0}^{(1)}(u, q)$, $\frac{dM_{c0}^{(2)}(u,q)}{du}$ (*line*) as obtained by [21] and as obtained by the RCWA algorithm (*line and dot*). The plots in Figs. 4 and 5 have been made over the entire Reg. 2 radial interval $\rho = 20$, $u_a \leq u \leq u_b$. As can be seen from Figs. 3–5, extremely close agreement exists between the Mathieu functions as obtained by RCWA method and by the numerical algorithm of [21] over the angular and radial intervals displayed.

We will now present numerical results of the EM fields which resulted for the two cases under consideration. Fig. 6 shows a plot of $\eta_0 H_{vR}$ ($\eta_0 = 377\Omega$, H_{vR} is the real part of the phasor magnetic field the H_v) for interval $\rho = 20$, $0 < u \leq 1.8$ with $v = 70°$ (an x-y
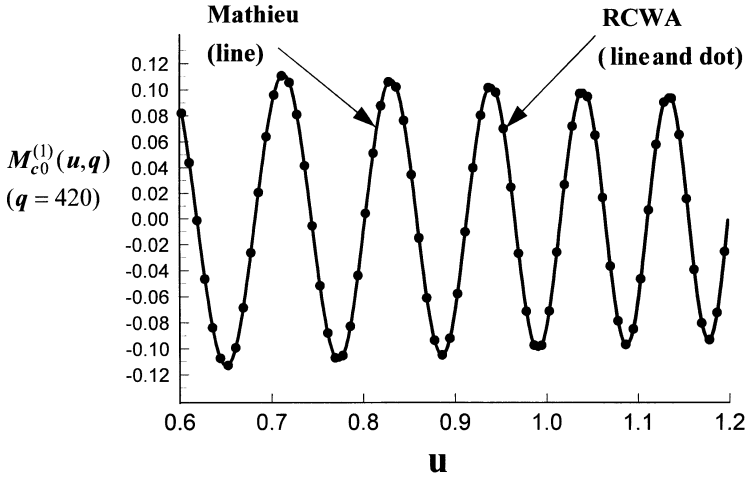
Figure 4. A comparison of the $M_{c0}^{(1)}(u,q)$ radial Mathieu function as calculated by [21] and as calculated by RCWA is shown for $q = 420$.
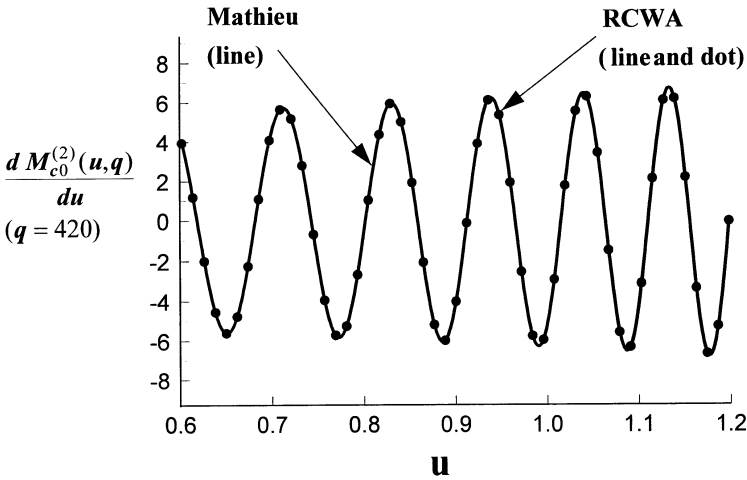

Figure 5. A comparison of the $\frac{dM_{c0}^{(2)}(u,q)}{du}$ radial Mathieu function as calculated by [21] and as calculated by RCWA is shown for $q = 420$.

Uniform Elliptical Cylinder   (**v** = 70°)
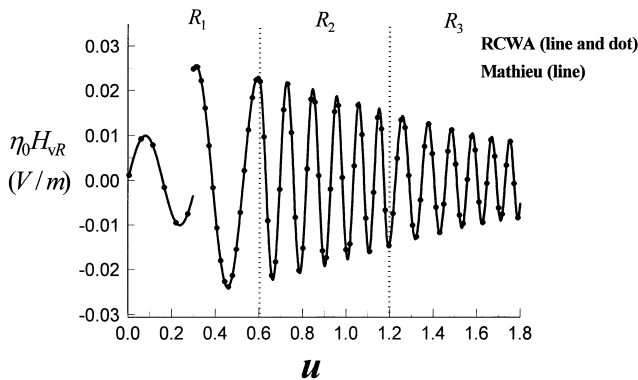
Figure 6. A comparison of $\eta_0 H_{vR}$ ($\eta_0 = 377\Omega$, H_{vR} is the real part of the phasor magnetic field the H_v) for interval $\rho = 20$, $0 < u \le 1.8$ with $v = 70°$ as obtained by a Mathieu expansion method of Sec. 3 and as obtained by RCWA algorithm of Sec. 2. Please see Fig. 2 for an x-y line plot of u for $\rho = 20$, $v = 70°$.

line plot of $v = 70°$ is shown in Fig. 2, *dashed* curve) as obtained by a Mathieu function expansion of Sec. 3 (*line*) and as obtained by the RCWA algorithm of Sec. 2 (*line and dot*). The discontinuous behavior of the plot at $u = .3$ in Reg. 1 is caused by the presence of the surface current Eq. (35) located at $u = u_s = .3$. As can be seen, extremely close agreement exists between the Mathieu and RCWA solution methods.

Figs. 7a–h for uniform and step profile cases, display the real and imaginary parts of the electric and magnetic fields over the interval $0 \le v \le \pi$ as calculated at radial values which are just above and just below the region interfaces values u_a and u_b. In these plots the EM fields for the uniform elliptical case set (*dashed* curves) were calculated using the Mathieu matching method of Sec. 3 and using the RCWA method of Sec. 2. Each set of dashed curves in Figs. 7a–h represents a set four curves (RCWA and Mathieu at u_a^- and u_a^+ Figs. 7a–d) or (RCWA and Mathieu at u_b^- and u_b^+, Figs. 7e–h). As can be seen from the dashed line plots of Figs. 7a–h, the Mathieu and RCWA methods give close agreement with each other. We also notice that the Mathieu and RCWA methods each method separately gives extremely close boundary matching agreement at the interfaces.

In the plots of Figs. 7a–h the EM results of the inhomogeneous, step profile case were studied using only the RCWA method of Sec. 2. Only the RCWA method was used since the Mathieu matching solution
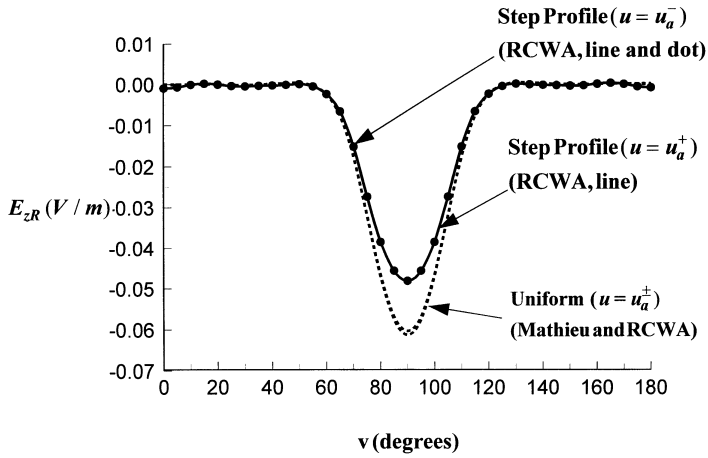
(a)
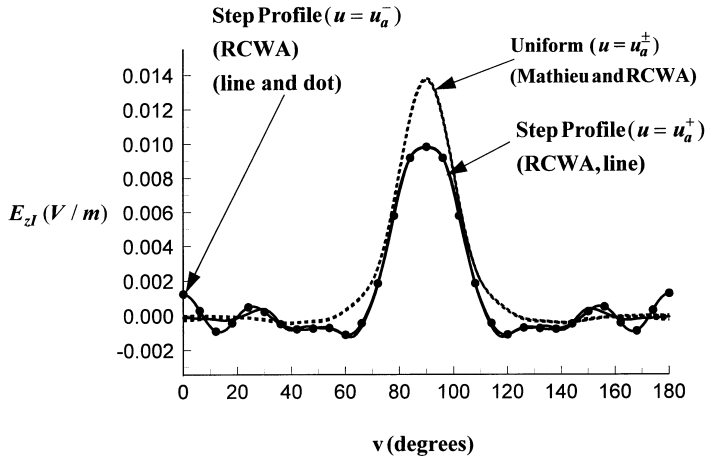
(b)

Figure 7. For uniform and step profile cases, Figs. 7a–h display the real (denoted by subscript R) and imaginary (denoted by subscript I) parts of the electric (E_z) and magnetic (H_v) fields over the interval $0 \leq v \leq 180°$ as calculated at radial values which are just above and just below the region interfaces values u_a and u_b.

Step Profile ($u = u_a^-$)
(RCWA, line and dot)

Step Profile ($u = u_a^+$)
(RCWA, line)

Uniform ($u = u_a^{\pm}$)
(Mathieu and RCWA)
(dashed)

$\eta_0 H_{vR}$
(V/m)

v (degrees)

(c)

Uniform ($u = u_a^{\pm}$)
(Mathieu and RCWA)

Step Profile ($u = u_a^+$)
(RCWA, line)

Step Profile ($u = u_a^-$)
(RCWA)
(line and dot)

$\eta_0 H_{vI}$
(V/m)

v (degrees)

(d)

Uniform ($u = u_b^{\pm}$)
(RCWA)

Uniform ($u = u_b^{\pm}$)
(Mathieu)

Step Profile ($u = u_b^-$)
(RCWA, line)

Step Profile ($u = u_b^+$)
(RCWA, line and dot)

$E_{zR} (V/m)$

v (degrees)
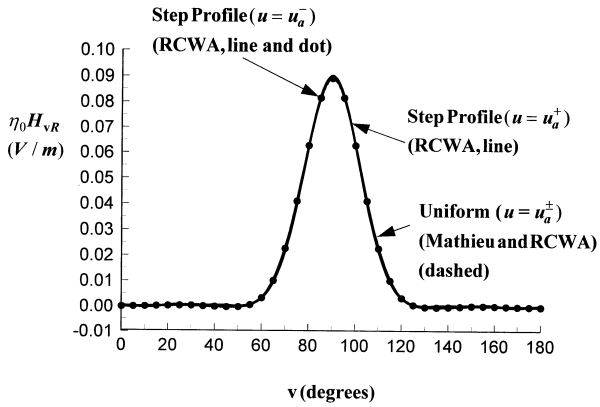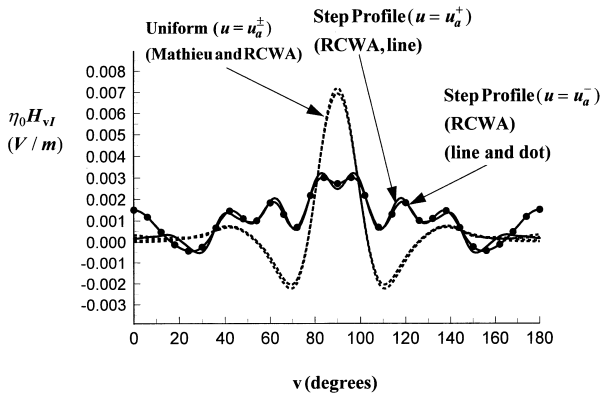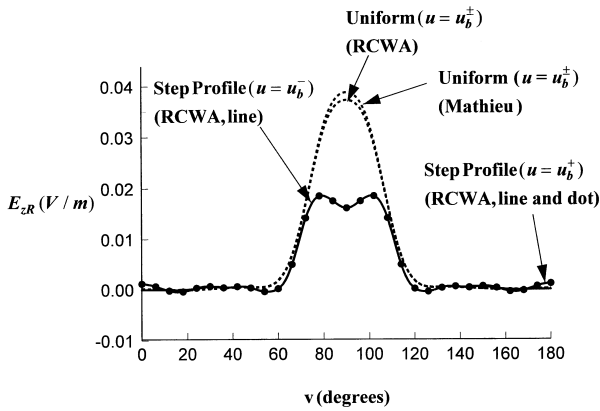
(e)
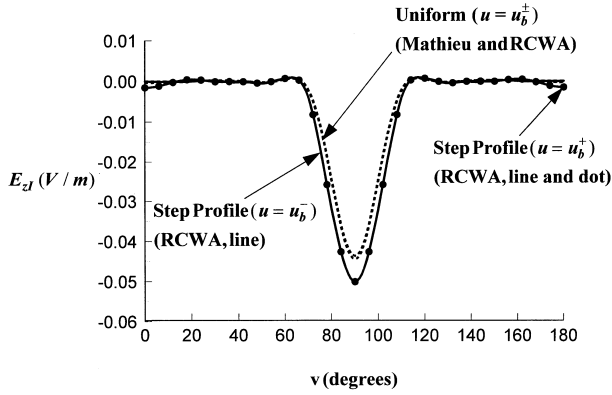
Figure 7.

(f)
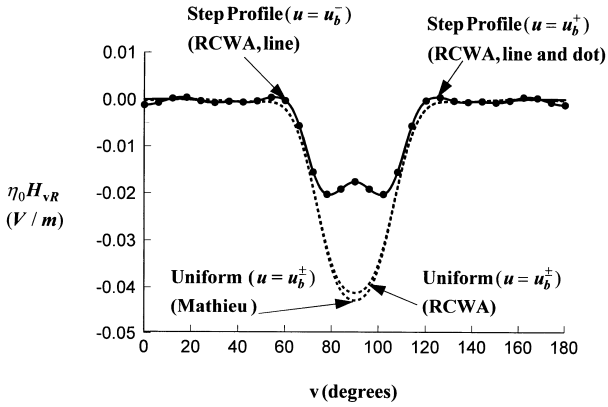
(g)
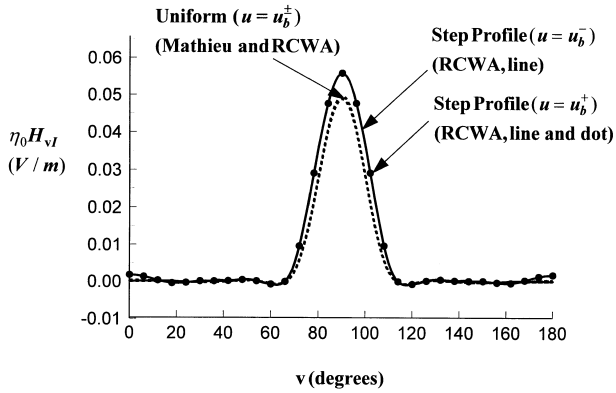
(h)

Figure 7.

described in Sec. 3 applies only to the uniform elliptical shell case. In these figures the EM fields of the RCWA method which were exterior to Reg. 2 (either u_a^- or u_b^+) were plotted as a solid *line and dot* and the EM fields which were interior to region 2 (either u_a^+ or u_b^- were plotted as a solid *line.* In observing the RCWA EM step profile results we notice that the numerical solutions satisfy EM boundary conditions fairly closely as there is little difference in the curves marked *line* and *line and dot.*

It is interesting to compare the EM results for the uniform and step profile cases. As can be seen from Figs. 7a–h, despite the fact that the two profiles had the same overall bulk dielectric value in Reg. 2, one notices that in all but Fig. 7c that two fairly significant differences occurred between the EM fields (both electric and magnetic) for the two cases under consideration. The first difference was that the magnitude of the peak EM field value which occurs at $v = 90°$ was smaller than the peak magnitude in the uniform case. The second major difference between the profiles was that the EM fields of step profile showed a much greater interference pattern over the $0 \leq v \leq 180°$ range than did the uniform shell example. Both of the differences in the EM field patterns are reasonable. The reduction in peak magnitude for the step profile is probably a dielectric bulk effect caused by the fact that in the step profile case, a large amount of the incident power of the current source (largest at $v = 90°$) encountered the Reg. 2b dielectric ($\varepsilon_{2b} = 3.05$). This dielectric region thus acted as if were the overall bulk dielectric of the entire elliptic shell. The second difference the interference effect is caused by the EM fields of the system being diffracted, reflected, and refracted from the discontinuities of step profile and subsequently interfering with one another to form the oscillatory EM field patterns seen in most of the RCWA plots of Figs. 7a–h.

In addition to the EM field results, calculations have been made of both the total power per unit length which is radiated from the system at any radial coordinate u in space and the power per unit length which is radiated from the different Mathieu orders ($m = 0, 2, \ldots$) at any radial coordinate u which is located in Regs. 1 or 3. The total, time averaged EM power radiated through a given elliptical shell located at any radial coordinate u is found by integrating

$$P_{TOT} = \int_0^{2\pi} .5\mathrm{Real}\left(\vec{E} \times \vec{H}^*\right) \cdot \hat{a}_u h(u, v) dv \qquad (36)$$

(Poynting vector power) where $\vec{E}$ and $\vec{H}$ are the electric and magnetic fields obtained from the RCWA or Mathieu matching methods, and $\vec{H}^*$ is the complex conjugate $\vec{H}$. The power per unit length which

Table 1. The power ratio P_{TOT}/P_{JS} as calculated at u_a^-, u_a^+, u_b^- and u_b^+ for the uniform elliptical shell case as calculated by the RCWA method (first column), the uniform elliptical shell case as calculated by the Mathieu matching (second column), and the step profile case as calculated by the RCWA method (third column) is shown. When Reg. 1 is infinite and $\varepsilon_1 = 1., \mu_1 = 1.$, it turns out that the total power radiated form $\vec{J}_S(u_s, v)$ of Eq. (35) is $P_{JS} = 6.816674 \times 10^{-2}$ (Watts/m).

Power u	P_{TOT}/P_{JS} (RCWA, Uniform)	P_{TOT}/P_{JS} (Mathieu, Uniform)	P_{TOT}/P_{JS} (RCWA, Step Profile)
$u = u_a^-$ (Reg. 1)	0.7172154	0.7270283	0.586915
$u = u_a^+$ (Reg. 2)	0.7172139	0.7270261	0.5936726
$u = u_b^-$ (Reg. 2)	0.7172139	0.7270261	0.5936726
$u = u_b^+$ (Reg. 3)	0.7172258	0.727046	0.5940894

is radiated from the different Mathieu orders $(m = 0, 2, \ldots)$ at any radial coordinate u which is located in Regs. 1 or 3 is calculated by substituting the Mathieu function expansions that apply in Reg. 1 or 3 into Eq. (36) and then using the orthogonality of the Mathiueu functions to identify the order power for each m.

Table 1 displays the power ratio P_{TOT}/P_{JS}. as calculated at u_a^-, u_a^+, u_b^-, and u_b^+ for the uniform elliptical shell case as calculated by the RCWA method (first column), the uniform elliptical shell case as calculated by the Mathieu matching (second column), and the step profile case as calculated by the RCWA method (third column) where P_{JS} (also calculated using Eq. (36)) represents the total power per unit length associated with the case when the current source of Eq. (35) radiates into an infinite space with material parameters ε_1, μ_1. For the case when Reg. 1 is infinite and $\varepsilon = 1., \mu_1 = 1.$, it turns out that the total power radiated form $\vec{J}_S(u_s, v)$ of Eq. (35) is $P_{JS} = 6.816674 \times 10^{-2}$ (Watts/m) . As can be seen from Table 1, close agreement exists in the power ratio that was calculated at u_a^-, u_a^+, u_b^-, and u_b^+ for each column, thus showing that conservation of power holds numerically as it should. We also notice that the power ratio of the RCWA method (column 1) and the Mathieu matching method (column 2) agreed reasonably well for the uniform elliptical shell case. It is further noticed from Table 1 that the power ratio for the step profile case (calculated by the RCWA method) was significantly different (about 20% smaller) than the power ratio that resulted for the uniform elliptical shell case (calculated by RCWA or Mathieu matching). This is an interesting result considering

Power of Mathieu Orders

(Reg 3, $u = u_b^+$)

P_m / P_{JS} **(db)**

Step Profile
(RCWA, square)

Uniform (RCWA, circle)

Uniform (Mathieu, triangle)
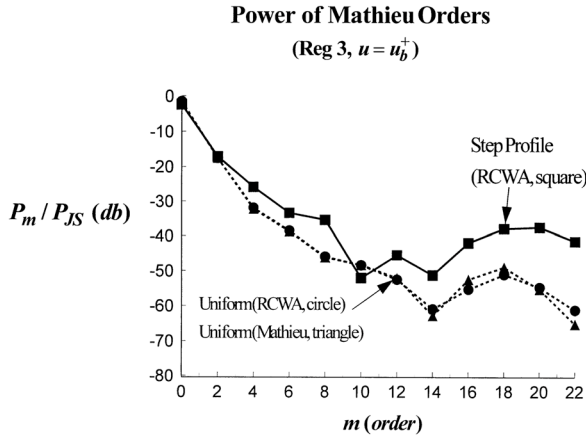
m (*order*)

Figure 8. A display of the power ratio in db (using the db power formula $10 \log(P_m/P_{JS})$) of the different Mathieu orders ($m = 0, 2, 4, \ldots, 22$) for the uniform elliptical shell case (using the Mathieu matching and RCWA methods) and the step profile case (RCWA) calculated in Reg. 3 at $u = u_b^+$ is shown. When Reg. 1 is infinite and $\varepsilon_1 = 1.$, $\mu_1 = 1.$, it turns out that the total power radiated form $\vec{J}_S(u_s, v)$ of Eq. (35) is $P_{JS} = 6.816674 \times 10^{-2}$ (Watts/m).

that uniform and step profile cases both had the same average or bulk dielectric value. The fact that the step and uniform profile cases had significantly different power ratios is not surprising, however, when one views the EM fields of Figs 7a–h. and one notices how different the EM fields of the two cases were.

Fig. 8 displays the power ratio in *db* (using the *db* power formula $10 \log(P_m/P_{JS})$) of the different Mathieu orders ($m = 0, 2, 4, \ldots, 22$) for the uniform elliptical shell case (using the Mathieu matching and RCWA methods) and the step profile case (RCWA) calculated in Reg. 3 at $u = u_b^+$. As can be seen from this figure for uniform shell case, the RCWA and Mathieu matching method give very close agreement to each other for the all the Mathieu orders. Also as can be seen from Fig. 8, the power ratio of most of the Mathieu orders for the step profile is much greater (from 6 to 20 db greater) than the Mathieu orders that result from the uniform elliptical shell. This indicates that the presence of the step profile causes a much higher rate of diffraction of the incident wave (EM radiation form the elliptical current source) into higher orders than is caused when only a uniform elliptical shells make up the system. This is a very reasonable result as one would expect the sharp discontinuities of the step profile to diffract EM field power into higher orders as it transits the elliptical shell region.

5. SUMMARY AND CONCLUSIONS

The RCWA method has been applied for the first time to study the problem of EM scattering and diffraction that occurs in an inhomogeneous dielectric elliptical, cylindrical system. Sec. 2 presented the RCWA algorithm, including the state variable formulation in the inhomogeneous dielectric region and the boundary-matching algorithm used. Sec. 3 presented a Mathieu function expansion method which was useful for determining the EM scattering and diffraction that occurs in a three region elliptical system when each of the regions was made up of a homogeneous dielectric material. The Mathieu function expansion method (applicable only to EM scattering problems involving uniform elliptical shells) provided an independent method with which to validate the RCWA numerical results (RCWA applies to homogeneous and inhomogeneous dielectric profiles). In Sec. 4 the RCWA and Mathieu matching algorithms were both used to determine the EM fields that result when a uniform elliptical shell was illuminated by an interior surface current, and the RCWA algorithm alone was used to determine the EM fields that result when a step profile was illuminated by an interior current. The permittivity of the uniform shell example was chosen to equal the bulk value step profile example in order that a useful comparison of the uniform and step profile examples could be made.

Several comments and conclusions can be reached about the numerical results of Sec. 4. First, as can be seen from inspection of Figs. 3, 4,and 5 the RCWA and Mathieu methods gave close agreement to each in the calculation of the angular and radial Mathieu functions for argument values which were displayed. Second, as can be seen from an inspection of Fig. 6, Fig. 7 (dashed curves), Fig. 8 and Table I (first two columns), the RCWA and Mathieu methods gave close agreement to each other in the calculation of the EM fields and power of the uniform profile example. Third, as can be seen from an inspection of Figs. 7 and 8 and Table 1 (columns 1 and 2 compared to column 3), the EM fields of the step profile example and uniform profile examples turned out to be different from one another, despite the fact that the same bulk permittivity values were used. An inspection of the Mathieu power orders in Fig. 8 shows that that more EM power is being diffracted into higher orders for the step profile example than as occurs for uniform example. Fourth as be seen from an inspection of Table 1, one observes that for both the RCWA and Mathieu methods that the conservation of power law holds to a fairly high degree.

In conclusion it seems that the RCWA algorithm is an effective way to solve EM elliptical scattering problems. Important future

research work that still remains is to apply the RCWA algorithm to more severe inhomogeneity problems and to study the case of scattering when a plane wave is incidence on an elliptical, inhomogeneous, scattering object.

REFERENCES

1. Bhartia, P., L. Shafai, and M. Hamid, "Scattering by an imperfectly conducting conductor with a radially inhomogeneous dielectric coating," *Int. J. Electron.,* Vol. 31, 531–535, 1971.

2. Kishk, A. A., R. P. Parrikar, and A. Z. Elsherbeni, "Electromagnetic scattering from an eccentric multilayered circular cylinder," *IEEE Trans. Antennas Propagat.,* Vol. 40, No. 3, 295–303, 1992.

3. Elsherbeni, A. Z. and M. Hamid, "Scattering by a cylindrical dielectric shell with inhomogeneous permittivity profile," *Int. J. Electronics,* Vol. 58, No. 6, 949–962, 1985.

4. Elsherbeni, A. Z. and M. Hamid. "Scattering by a cylindrical dielectric shell with radial and azimuthal permittivity profiles," *Proc. 1985 Symp. of Microwave Technology in Industrial Development,* (Invited), 77–80, Brazil, July 22–25, 1985.

5. Elsherbeni, A. Z. and M. Tew, "Electromagnetic scattering from a circular cylinder of homogeneous dielectric coated by a dielectric shell with a permittivity profile in the radial and azimuthal directions-even TM case," *IEEE Proceedings-1990 Southeastcon,* Session 11A1, 996–1000, 1990.

6. Jarem, J. M., "Rigorous coupled wave theory solution of phi-periodic circular cylindrical dielectric systems," *Journal of Electromagnetic Waves and Applications,* Vol. 11, 197–213, 1997.

7. Jarem, J. M., "Rigorous coupled wave theory of anisotropic, azimuthally-inhomogeneous, cylindrical systems," *Progress in Electromagnetics Research,* PIER 19, Chap. 4, 109–127, 1998.

8. Jarem, J. M. and P. P. Banerjee, "Bioelectromagnetics: A rigorous coupled wave analysis of cylindrical biological tissue," *Proceedings of the International Conference on Mathematics and Engineering Techniques in Medicine and Biological Sciences, (METMBS 00),* F. Valatar (Ed.), 467–472, Vol. II, Las Vegas, Nev., June 26–29, 2000.

9. Moharam, M. G. and T. K. Gaylord, "Rigorous coupled-wave analysis of planar grating diffraction," *J. Opt. Soc. Amer.,* Vol. 71, 811–818. 1981.

10. Moharam, M. G. and T. K. Gaylord, "Diffraction analysis of

dielectric surface-relief gratings," *J. Opt. Soc. Amer.,* Vol. 72, 1385–1392, 1982.

11. Rokushima, K. and J. Yamakita, "Analysis of anisotropic dielectric gratings," *J Opt. Soc. Amer.,* Vol. 73, 901–908, 1983.

12. Moharam, M. G. and T. K. Gaylord, "Three-dimensional vector coupled-wave analysis of planar-grating diffraction," *J. opt. Soc. Amer.,* Vol. 73, 1105–1112, 1983.

13. Glytsis, E. N. and T. K. Gaylord, "Rigorous three-dimensional coupled-wave diffraction analysis of single cascaded anisotropic gratings," *J Opt. Soc. Amer. B,* Vol. 4, 2061–2080, 1987.

14. Jarem, J. M. and P. Banerjee, "An exact, dynamical analysis of the Kukhtarev equations in photoretractive barium titanate using rigorous wave coupled wave diffraction theory," *J. opt. Soc. Amer. A,* Vol. 13, No. 4, 819–831, April 1996.

15. Jarem, J. M., "A rigorous coupled-wave theory and crossed-diffraction grating analysis of radiation and scattering from three-dimensional inhomogeneous objects," a Letter, *IEEE Transactions on Antennas and Propagation,* No. 5, Vol. 46, 740–741, May 1998.

16. Jarem, J. M., "Rigorous coupled-wave-theory analysis of dipole scattering from a three-dimensional, inhomogeneous, spherical dielectric and permeable system," *IEEE Microwave Theory and Techniques,* Vol. 45, No. 8, 1193–1203, Aug. 1997.

17. Jarem, J. M. and P. P. Banerjee, *Computational Methods for Electromagnetic and Optical Systems,* Marcel Dekker, Inc., 2000.

18. Bowman, J. J., T. B. Senior, and P. L. E. Uslenghi, *Electromagnetic and Acoustic Scattering by Simple Shapes,* Chap. 3. "The Elliptic Cylinder", 129–180, Hemisphere Publishing Corp., New York, N.Y., revised printing, 1987.

19. Sebak, A. R., "Scattering from Dielectric-Coated Impedance elliptic cylinder," *IEEE Transactions on Antennas and Propagation,* Vol. 48, No. 10, 1574–1580, Oct. 2000.

20. Abramowitz, M. and I. Stegum, *Handbook of Mathematical Functions,* Chap. 20, "Mathieu Functions", Dover publications, New York, N.Y., 1972.

21. Zhang, S. and J. Jin, "FORTRAN routines for computation of special functions," Programs: "MTU12,MTU0,FCOEF,CVF, CVA2" at Web Site http://irislee3.ece.uiuc.edu/~jjin/routines/routines.html, Mar. 8, 01. (Programs associated with the book *Computation of Special Functions,* John Wiley and Sons. Inc.)